# Synthesis of Hollow Poly(aniline-*co*-pyrrole)-$Fe_3O_4$ Composite Nanospheres and their Microwave Absorption Behavior

Yao-Feng Zhu[a], Li Zhang[b], Toshiaki Natsuki[c], Ya-Qin Fu[d], Qing-Qing Ni[c,d*]

[a] Interdisciplinary Graduate School of Science and Technology, Shinshu University, Tokida, Ueda 386-8576, Japan

[b] Faculty of Engineering, Shinshu University, Wakasato, Nagano 380-8553, Japan

[c] Department of Functional Machinery & Mechanics, Shinshu University, Tokida, Ueda 386-8576, Japan

[d] Key Laboratory of Advanced Textile Materials and Manufacturing Technology Ministry of Education, Zhejiang Sci-Tech University, Hangzhou 310018, P.R. China

**Abstract**

Hollow poly(aniline-*co*-pyrrole)-$Fe_3O_4$ (HPAP-$Fe_3O_4$) nanospheres with significant electromagnetic properties were successfully prepared via the oxidative polymerization of a mixture of aniline and pyrrole in the presence of a magnetic fluid, using a non-ionic surfactant as a template. The products were characterized by field emission scanning electron microscopy, transmission electron microscopy, Fourier transform infrared spectroscopy, X-ray powder diffraction, thermogravimetric analysis and X-ray photoelectron spectroscopy. The electromagnetic (EM) and microwave absorbing properties of the nanocomposites were also investigated. The HPAP-$Fe_3O_4$ nanospheres exhibit superparamagnetic properties, and the conductivity increases with $Fe_3O_4$ content. The reflection loss evaluation based on the absorbing wall theory at 2 mm thickness shows that the reflection loss is reinforced in the frequency range of 0.5-10 GHz by the presence of $Fe_3O_4$ nanoparticles, and the frequency of minimum reflection loss shifts to a higher value with increasing $Fe_3O_4$ content. HPAP-$Fe_{06}$ exhibits the best microwave absorbing property between 0.5 and 10 GHz.

*Corresponding author at: Department of Functional Machinery & Mechanics, Shinshu University, 3-15-1 Tokida, Ueda 386-8567, Japan. Tel/Fax: +81 268 21 5438

E-mail address: niqq@shinshu-u.ac.jp (Qing-Qing Ni)

**Keywords:** Copolymer; Magnetite; Nanospheres; Hollow structures; Microwave absorbing property

## 1. Introduction

The rapid development of gigahertz (GHz) electronic systems for telecommunications and defense applications has led to serious EM interference problems and thus a requirement for EM wave absorbing materials with effective shielding over a broad band of frequencies and preferably with a low density [1-3]. EM functionalized conducting polymer composites with micro/nanostructures are considered good candidate materials for EM wave absorption because their microwave properties can be improved by both magnetic and dielectric losses, which are expected to lead to microwave absorption over a broad range of frequencies [4-6].

Conductive polymers play an important role in technologies such as those requiring “stealth”, electrostatic charge dissipation and EM interference shielding [1]. Among them, polyaniline (PANI) and polypyrrole (PYY) are promising materials for practical applications because of their controllable conductivity, environmental stability, ease of preparation and favorable physiochemical properties, In addition, the inorganic magnetic micro/nanoparticles can co-structure with a monomer to form micro/nanostructured composites via a self-assembly process [7-11]. $Fe_3O_4$ nanoparticles have unique magnetic properties and facile synthesis routes. It is also reported that $Fe_3O_4$ nanoparticles exhibit excellent microwave absorption at low frequencies, which is particularly relevant to magnetic loss[12]. Therefore we have prepared $Fe_3O_4$-conducting polymer composite materials because their microwave absorption properties are likely to be improved by both magnetic and dielectric loss mechanisms. Recently, Deng et al synthesized $Fe_3O_4$ cross-linked PAni nanoparticles that exhibited high magnetization and conductivity [13]. Phang et al prepared hexanoic acid doped PAni nanocomposites containing $TiO_2$ and $Fe_3O_4$ that have excellent microwave absorption performance [14]. He et al synthesized PANI/CIP/$Fe_3O_4$ composites that have good EM wave absorption at high frequencies [4]. However, the preparation of EM functionalized conducting polymer composites has not yet been reported in detail. Composite properties are dependent on structure and component size, so the synthesis of composite nanostructures with well defined component size and morphology is of great interest. Despite all the

progress in the synthesis of $Fe_3O_4$-conducting polymer nanospecies with various structures, the controllable and selective fabrication of $Fe_3O_4$-conducting polymers nanomaterials of a particular desired shape is still a challenge.

In this paper, the main objective is to design a microwave absorbing composite material with controllable nanostructure. Hollow nanospheres have a wide range of potential applications [15-17], but the preparation of EM functionalized copolymer hollow structures has not yet been reported. Hollow poly(aniline-*co*-pyrrole)-$Fe_3O_4$ (HPAP-$Fe_3O_4$) nanosphere composites were synthesized by the oxidative polymerization of a mixture of aniline and pyrrole in the presence of a magnetic fluid, using a non-ionic surfactant as a template. The morphology and molecular structure of the composite hollow nanospheres were investigated in detail, as was the correlation between electrical and magnetic properties with microwave absorption.

## 2. Experimental

### 2.1 Materials

Aniline (99%) was supplied by Wako Pure Chemical Reagent Co., Ltd., Japan). Pyrrole (98%, by Sigma Aldrich, Co., Ltd., USA) and was stored below 0°C. Sodium dodecyl sulfate, polyoxyethylene(10) octylphenyl ether (Triton X-100), ammonium peroxodisulfate, $FeCl_3 \cdot 6H_2O$, $FeCl_2 \cdot 4H_2O$, ammonia (28%), and ethanol (99.5%) were of analytical purity and were used as received. Deionized water was used throughout the experiments.

### 2.2 Synthesis of $Fe_3O_4$ nanoparticles

The $Fe_3O_4$ magnetic nanoparticles were prepared by a modified co-precipitation method. The reaction was carried out in a 250-ml three-necked round-bottom flask equipped with a stirrer. $FeCl_2 \cdot 4H_2O$ (0.994 g, 5 mmol) in 10 ml of deionized water and 2.73 g (10 mmol) of $FeCl_3.6H_2O$ in 10 ml of deionized water were mixed by vigorous stirring and the mixed solution kept in a water bath at 80°C. Twenty milliliters of preheated ammonia solution (1.5 M) was added rapidly to the solution, followed by dropwise addition of aqueous ammonia with stirring until the pH reached 10-12, and stirring was then continued for 1 h. The $Fe_3O_4$ nanoparticles formed were collected by

magnetic field separation, washed three times with deionized water, and dried under vacuum at 50°C for 24 h.

2.3 Synthesis of HPAP-$Fe_3O_4$ nanospheres with hollow structure

Hollow poly(aniline-co-pyrrole)-$Fe_3O_4$ (HPAP-$Fe_3O_4$) nanospheres were prepared via *in situ* emulsion polymerization in an aqueous solution containing $Fe_3O_4$ magnetic fluid and a surfactant. A typical synthesis for HPAP-$Fe_3O_4$ nanospheres was as follows. A known amount of $Fe_3O_4$ nanoparticles were mixed with a known amount of surfactant (sodium dodecyl sulfate) dispersed in 20 ml of deionized water with ultrasonication for 2.5 h to obtain a uniform magnetic fluid. Then 1 mmol of pyrrole was added and the suspension was ultrasonicated for 0.5 h. Aniline (1 mmol) and 0.02 g Triton X-100 were added and the mixture ultrasonicated for a further 0.5 h. The mixture was maintained at 0-5°C for 0.5 h, and then 0.2 mmol of ammonium peroxodisulfate was added to initiate polymerization, which took place at 0-5°C for 24 h without agitation. The resulting product was collected by filtration and thoroughly washed with a mixture of deionized water, 95% ethanol, and 0.1 M HCl until the filtrate became colorless. Finally, the hollow poly(aniline-*co*-pyrrole)-$Fe_3O_4$ nanospheres were vacuum-dried at 50°C for 24 h. By varying the amount of the $Fe_3O_4$ magnetic nanoparticles used (0.01 g, 0.02 g, 0.04 g, and 0.06 g), different products were obtained, and these were designated as HPAP-$Fe_{01}$, HPAP-$Fe_{02}$, HPAP-$Fe_{04}$, and HPAP-$Fe_{06}$. As a control, HPAP nanospheres were prepared in the absence of $Fe_3O_4$ nanoparticles via *in situ* emulsion polymerization as described above.

2.4 Characterization

The morphology of the products was investigated using field emission scanning electron microscopy (FE-SEM; JEOL S-5000) and transmission electron microscopy (TEM; JEOL JEM-2010). X-ray powder diffraction (XRD) patterns were obtained with a RINT 2550H diffractometer using Cu Kα radiation. Fourier transform infrared spectroscopy (FT-IR) spectra of KBr powder pressed samples were recorded in the range 400-4000 $cm^{-1}$ with a Shimadzu IR-prestige21 spectrometer. Thermogravimetric analysis (TGA; TG8120, Rigaku Denki) was

carried out under an air atmosphere from 50 to 600°C at a heating rate of 5°C $min^{-1}$, then a soak at 600°C for 30 min. X-ray photoelectron spectroscopy (XPS) was performed using a Kratos Axis Ultra DLD X-ray spectrometer with Mg as the exciting source. The room-temperature conductivity of the nanocomposites formed under 30MPa was measured according to a standard four-probe method using a MCP-HT450 conductivity meter (Dia-instruments Co., Ltd.). Magnetic measurements were carried out at room temperature using a vibrating sample magnetometer (TM-VSM5250, Japan) with a maximum magnetic field of 10 KOe.

The samples used for measurement of microwave properties were prepared by dispersing the poly(aniline-*co*-pyrrole)-$Fe_3O_4$ nanocomposite powder in paraffin wax. The powder-wax compound was pressed into a toroidal shape with an outer diameter of 7 mm, inner diameter of 3.0 mm and a thickness of 2 mm. The complex permittivity and permeability of the compound samples were measured using a vector network analyzer (37247D Anritsu Co., Ltd.) over a range of 0.5-10 GHz, and the reflection loss was calculated from the measured complex permittivity and permeability.

## 3. Results and discussion

### 3.1 Morphology and structure of HPAP-$Fe_3O_4$ nanospheres

A TEM image of $Fe_3O_4$ nanoparticles is shown in Fig. 1. The $Fe_3O_4$ nanoparticles were almost uniform in shape and size, at about 10 nm in average diameter, and were relatively well dispersed. The enlarged TEM image in the inset to Fig. 1 suggests that the nanoparticles were well crystallized. FE-SEM images of the HPAP nanospheres and HPAP-$Fe_{04}$ nanospheres (Fig. 2 (a) and (b)) show that the samples were uniform spheres with an average diameter of about 100 nm. From the insets (magnified FE-SEM images) it is clear that the HPAP nanospheres had smooth surfaces, while the surfaces of the HPAP-$Fe_{04}$ nanospheres were relatively rough. The TEM images of HPAP nanospheres and HPAP-$Fe_{04}$ nanospheres in Fig. 2 (c) and (d) reveal that the samples had hollow interiors. The TEM images also show that the average shell thickness was in the range 20-30 nm. From Fig. 2 (d) it is clear that the $Fe_3O_4$ nanoparticles were encapsulated in the compound nanospheres, causing the rough surface.

Figure 4 shows XRD patterns from HPAP nanospheres (Fig. 3(a)), HPAP-$Fe_3O_4$ nanospheres (Fig. 3 (b-e)) and $Fe_3O_4$ nanoparticles (Fig. 3(f)). The single broad band centered at around 21° for the HPAP nanospheres (Fig. 3(a)) is indicative of an amorphous structure, arising from the interaction between the different components [8,18]. The broad band centered at around 21° was also observed for HPAP-$Fe_3O_4$ nanospheres (Fig. 3 (b-e)), together with diffraction peaks at 2θ=30.1°, 35.5°, 43.3°, 53.6°, 57.2° and 62.7° that are in agreement with the XRD peaks of pure $Fe_3O_4$ nanoparticles (Fig. 3 (f)). The peaks correspond to the (220), (311), (400), (422), (511), and (440) Bragg reflections characteristic of $Fe_3O_4$, confirming that the HPAP-$Fe_3O_4$ nanospheres contained $Fe_3O_4$ nanoparticles. The results also indicate that the $Fe_3O_4$ nanoparticles had a cubic spinel structure identical to that of the reference material in the JCPDS file (PDF No. 65-3107) [19-21].

The molecular structure of the products was determined by FT-IR spectroscopy; sample spectra are shown in Fig. 4. Similar absorption bands were observed both for HPAP nanospheres (Fig. 4 (b)) and HPAP-$Fe_3O_4$ nanospheres (Fig. 4 (c-f)) at 1575, 1564, 1458, 1281, 1190 and 694 $cm^{-1}$. The bands at 1575 and 1564 $cm^{-1}$ correspond to the C-C stretch for the quinonoid phenyl rings of PANI and C=C stretching mode of polypyrrole [8, 22]. The peak at 1458 $cm^{-1}$ is attributed to benzenoid vibrations, and the bands at 1281 and 1190 $cm^{-1}$ are due to the presence of aromatic NH groups and the C-N stretching vibration [18, 23]. The band at 694 $cm^{-1}$ is attributed to C-H in-plane bending in the 1,3-substituted benzene ring, which may be induced by the attachment of pyrrole units at the *meta*-position of the benzene ring [24]. Figure 4(a) shows the FT-IR spectrum of $Fe_3O_4$ nanoparticles, with characteristic absorption $Fe_3O_4$ at 586 $cm^{-1}$ that is assigned to the Fe-O bond. The characteristic peak of $Fe_3O_4$ was not observed in the HPAP-$Fe_3O_4$ nanospheres, indicating that the $Fe_3O_4$ nanoparticles were fully encapsulated in the nanospheres.

XPS analysis gave some insight into the chemical composition of the composite nanospheres. Figure 5 (a) shows that the HPAP-$Fe_{04}$ nanospheres were composed mainly of C, N and O. The N 1s XPS core level spectrum of HPAP-$Fe_{04}$ nanospheres is shown in Fig. 5 (b). The N 1s signal was fitted by three sub-bands, corresponding to quinonoid imine (=N-) at 398.0 eV, benzenoid amine

(-NH-) at 398.9 eV, and positively charged nitrogen atoms with a binding energy of 399.6 eV. This result indicated coexistence of the pernigraniline and emeraldine states of the conducting polymer. However, the binding energies were shifted to lower energy and were slightly different from those reported previously [17,25]. The energy level shifts can be accounted for by the dehydrogenation of pyrrolylium nitrogen and rearrangement of the pyrrole bonds to satisfy the nitrogen valences, and interaction between N and Fe atoms to form a coordinate bond, which could reduce the energy level of the composite nanospheres [19,26]. The C 1s spectrum of HPAP-$Fe_{04}$ nanospheres displays a large peak centered at about 285 eV, as shown in Fig. 5 (c), which is attributed to the presence of aromatic carbons, quinoneimine units and charged species. In addition, the XPS spectra of HPAP-$Fe_{04}$ nanospheres show that no elemental Fe was present, confirming that the $Fe_3O_4$ nanoparticles were well encapsulated in the nanospheres. This result is in agreement with the FT-IR spectra and the morphology of the HPAP-$Fe_3O_4$ nanospheres.

TGA curves of the HPAP nanospheres and HPAP-$Fe_3O_4$ nanospheres are presented in Fig. 6. The HPAP nanospheres showed three stages of weight loss. The initial weight loss up to 100°C is due to the evaporation of water trapped in the sample. The gradual weight loss up to 280°C is attributed to loss of low molecular weight oligomer, and oxidative thermal degradation began above 300°C. The HPAP-$Fe_3O_4$ nanospheres showed similar decomposition steps to those of HPAP nanospheres, but the decomposition processes of the two samples above 300°C indicated that the HPAP-$Fe_3O_4$ nanospheres had lower thermal stability. The lower thermal stability of HPAP-$Fe_3O_4$ nanospheres may be due to the synthesis by *in situ* polymerization in the $Fe_3O_4$ magnetic fluid, which leads to the presence of polymer chain defects and a consequent broad molecular weight distribution. From the TGA trace of the HPAP-$Fe_3O_4$ nanospheres, we believe that the weight loss could be assigned to polymer decomposition. Meanwhile, $Fe_3O_4$ oxidized to form $Fe_2O_3$, and the $Fe_2O_3$ mass percentage and the $Fe_3O_4$ contents are then derived from the $Fe_2O_3$ mass percentage, as shown in Table 1.

3.2 Magnetic and electrical properties

The presence of $Fe_3O_4$ is the reason for the EM functionalization of the composite nanoparticles, so

the magnetic properties of $Fe_3O_4$ and HPAP-$Fe_3O_4$ nanospheres were measured using a vibrating sample magnetometer at room temperature with an applied field -10 KOe$\leqq H \leqq$10 KOe. As shown in Fig. 7, the saturated magnetization of pure $Fe_3O_4$ nanoparticles was about 59.6 emu/g. The saturated magnetization of the HPAP-$Fe_3O_4$ nanospheres is affected by the amount of magnetic fluid present. The saturated magnetizations of HPAP-$Fe_{01}$, HPAP-$Fe_{02}$, HPAP-$Fe_{04}$, and HPAP-$Fe_{06}$ are 2.49, 4.99, 11.07, 17.2 emu/g. According to the TGA analyses, the $Fe_3O_4$ content of HPAP-$Fe_3O_4$ nanospheres increased with the increase in the amount of magnetic fluid added, and the results for the $Fe_3O_4$ mass percentage are shown in Table 1. The relationship between saturated magnetization and $Fe_3O_4$ content is obtained as shown in Fig. 8. The saturated magnetization of HPAP-$Fe_3O_4$ nanospheres increased linearly with $Fe_3O_4$ content. This indicates that the magnetic properties of the composites are mainly due to $Fe_3O_4$. The $Fe_3O_4$ and HPAP-$Fe_3O_4$ nanospheres have a low coercive force (*Hc*) (about 300 Oe). Therefore, this kind of composite could exhibit significant electric-magnetic absorption properties.

The electrical properties of HPAP and HPAP-$Fe_3O_4$ nanospheres were also examined. As shown in Fig. 9, the room temperature conductivity of the HPAP and HPAP-$Fe_3O_4$ nanospheres was measured by a four-probe method. It is found that the conductivity of the HPAP-$Fe_3O_4$ nanospheres was higher than that of the HPAP nanospheres. Furthermore, the conductivity of the HPAP- $Fe_3O_4$ nanospheres increased to some extent with $Fe_3O_4$ content, which has been previously observed [27,28]. The conductivity of HPAP-$Fe_3O_4$ nanospheres may be not only affected by the microscopic conductivity but could also be affected by macroscopic conductivity [27]. Microscopic conductivity depends upon the doping level, conjugation length and polymer chain length, which should not vary widely in samples prepared under identical conditions. Our HPAP-$Fe_3O_4$ nanospheres were polymerized in identical conditions, so the microscopic conductivities should be nearly the same. However, the macroscopic conductivity depends on certain external factors such as compaction of the samples or molecular orientation, which in turn significantly depend on the $Fe_3O_4$ content in the HPAP-$Fe_3O_4$ nanospheres. Pure co-polymer is poorly compacted, which results in relatively lower

conductivity. In the HPAP-$Fe_3O_4$ nanospheres, the growing polymer chains are supported on the $Fe_3O_4$ particles, which lead to an improvement in the compaction of the composite material. Therefore, as the $Fe_3O_4$ content increases, the compaction of the composites is significantly improved, which results in an enhancement in macroscopic conductivity measured in the pelletized form.

3.3 Microwave absorption properties

The complex permittivity of HPAP-$Fe_3O_4$ nanosphere-paraffin wax composites made with 50 wt% of HPAP-$Fe_3O_4$ is presented in Fig. 10 (a-b). The complex permittivity $\varepsilon$ ($\varepsilon=\varepsilon'-j\varepsilon''$) has real ($\varepsilon'$) and imaginary ($\varepsilon''$) permittivities. Figure 10 (a-b) shows the real and imaginary parts of the complex permittivity ($\varepsilon',\varepsilon''$) of the HPAP-$Fe_3O_4$-paraffin wax nanocomposites. As shown in Fig. 10 (a), the real part ($\varepsilon'$) of the permittivity of the samples increases with $Fe_3O_4$ content in the HPAP-$Fe_3O_4$ nanospheres, especially in the range of 0.5-6 GHz, while HPAP-$Fe_{06}$ is similar to HPAP-$Fe_{04}$ in the range of 0.5-2 GHz. Between 6 and 10 GHz, the $\varepsilon'$ of the samples is less sensitive to the $Fe_3O_4$ content, except in HPAP-$Fe_{06}$, which has a higher value. It is also found that the $\varepsilon'$ is critically dependent on the frequency and decreases in inverse proportion to the frequency. For the imaginary part of the permittivity $\varepsilon''$, it can be seen in Fig. 10 (b) that $\varepsilon''$ of the samples increases with the $Fe_3O_4$ content in the frequency of 3-8 GHz range and remains approximately constant between 8 and 10 GHz except in the HPAP-$Fe_{06}$ sample. It also can be seen that there is some cross-over of $\varepsilon''$ between HPAP-$Fe_{04}$ and HPAP-$Fe_{06}$ at low frequencies. $\varepsilon''$ exhibits four resonance peaks, lying at 1.5, 3.5, 5.5 and 7.5 GHz. These resonance peaks are usually attributed to interfacial polarization [29], which may be caused by the nature of the interface between the $Fe_3O_4$ nanoparticles and the co-polymer, and polarization by the $Fe_3O_4$ nanoparticles [30].

Figure 10 (c-d) shows the complex permeability of the HPAP-$Fe_3O_4$ nanosphere-paraffin wax composites with 50 wt% of HPAP-$Fe_3O_4$ in the frequency range of 0.5-10 GHz. The result for the real part ($\mu'$) of the complex permeability is shown in Fig. 10(c). It is found that $\mu'$ increases along with frequency. The samples have similar values below 5.5 GHz and have three resonance peaks in

the frequency of 4-10 GHz, implying normal resonance. The imaginary part ($\mu''$) of the complex permeability of the samples is shown in Fig. 10 (d). It is found that the $\mu''$ values of the samples increase with frequency, but sample HPAP-$Fe_{01}$ and HPAP-$Fe_{02}$ have a slight decrease at high frequencies. The $\mu''$ values of the samples have three resonance peaks near 5 GHz, 6.5 GHz and 8.5 GHz. The magnetic losses mainly consist of natural resonance, domain-wall displacement, magnetic hysteresis, and eddy current loss, and because the size of the $Fe_3O_4$ nanoparticles is far smaller than the skin depth (~1 $\mu$m), it may be that the microwave magnetic loss for the present HPAP-$Fe_3O_4$ nanospheres is mainly due to natural resonance of the $Fe_3O_4$ nanoparticles [31,32]. It is believed that natural resonance results in strong magnetic loss, implying enhanced microwave absorption by the HPAP-$Fe_3O_4$ nanospheres as EM energy is converted into heat energy [33].

To investigate the intrinsic reasons for microwave absorption by the HPAP-$Fe_3O_4$ nanospheres, the dielectric loss factor ($\tan\delta_E=\varepsilon''/\varepsilon'$) and the magnetic loss factor ($\tan\delta_M=\mu''/\mu'$) of sample HPAP-$Fe_{04}$ were calculated. It can be seen from Fig. 11 that both the dielectric and magnetic loss do contribute to microwave absorption. The magnetic loss factor is larger than the dielectric loss factor, and the total EM loss behavior is similar, if somewhat larger than that of magnetic loss. Thus the main contribution to microwave absorption comes from magnetic losses.

The reflection loss (*R.L.*) of the samples with thickness of 2 mm in 0.5-10 GHz was calculated, as shown in Fig. 12, according to transmission line theory [34], as:

$$R.L. = 20\log\left|\frac{Z_{in}-1}{Z_{in}+1}\right| \qquad (1)$$

$Z_{in}$ is the normalized input impedance of a metal-backed microwave absorbing layer.

$$Z_{in} = \sqrt{\frac{\mu_r}{\varepsilon_r}}\tanh\left[j\left(\frac{2\pi fd}{c}\right)\sqrt{\mu_r\varepsilon_r}\right] \qquad (2)$$

where $f$ is the microwave frequency in Hz, $d$ is the thickness of the absorber in m, and c is the velocity of light in free space in m/s.

It can be seen that the frequency for the minimum reflection loss decreases with increasing $Fe_3O_4$

content. Meanwhile, the increased reflection loss at higher frequency ranges is accompanied by attenuation at lower frequency bands. From the composites prepared in this study, HPAP-$Fe_{06}$ exhibits the best microwave absorbing property. The minimum reflection loss of HPAP-$Fe_{06}$ sample is about -3 dB at 9 GHz and 10 GHz when $d$=2 mm, which is higher than other reported results [29,35]. As the $Fe_3O_4$ content increases, the reflection loss peaks shift slightly towards higher frequency, which is consistent with previous reports [36]. Additionally, the magnetic and conductivity properties are enhanced by increasing the $Fe_3O_4$ content, as shown in Fig. 7 and Fig. 9, showing the distinct resulting change in both dielectric and magnetic loss, significantly affecting the efficiency of microwave absorption [37].

## 4. Conclusion

HPAP-$Fe_3O_4$ composite nanospheres with EM properties were successfully fabricated by oxidative polymerization of a mixture of aniline and pyrrole in the presence of a magnetic fluid, using a non-ionic surfactant as template. The HPAP-$Fe_3O_4$ composite nanospheres exhibited good conductivity and magnetic properties. The reflection loss in 0.5-10 GHz range of HPAP-$Fe_3O_4$ composite nanospheres was reinforced by the presence of $Fe_3O_4$ nanoparticles and the frequency relating to minimum reflection loss shifted to higher value with increased $Fe_3O_4$ content. The calculated result for the reflection loss also showed that the HPAP-$Fe_{06}$ sample had the best microwave absorbing property in the 0.5-10 GHz range. It is reasonable to believe that HPAP-$Fe_3O_4$ functional composites have potential applications in chemical sensors, gas separation, catalysis, microwave shielding, and magnetoelectric devices.

## Acknowledgments

This work was partly supported by grants-in-aid from the Global COE Program and CLUSTER (the second stage) by the Ministry of Education, Culture, Sports, Science and Technology, Japan

## References

[1] S. W. Phang, M. Tadokoro, J. Watanabe, N. Kuramoto. Curr. Appl. Phys. 8(2008) 391-394

[2] R.T. Ma, H.T. Zhao, G. Zhang. Mater. Res. Bull. 45(2010) 1064-1068

[3] T. H. Ting, K.-H. Wu. J. Magn. Magn. Mater. 322(2010) 2160–2166.

[4] Z.F. He, Y. Fang, X.J. Wang, H. Pang. Synth. Met. 161(2011)420-425

[5] G.Q. Wang, X.D. Chen, Y.P. Duan, S.H. Liu. J. Alloys Compd. 454(2008) 340-346

[6] D.L. Zhao, Q. Lv, Z.M. Shen. J. Alloys Compd. 480(2009)634-638

[7]C. Saravanan, R. C. Shekhar, S. Palaniappan. Macromol. Chem. Phys. 207(2006)342–348

[8]S. E. Mavundla, G. F. Malgas, D. E. Motaung, E. I. Iwuoha. J. Mater. Sci. 45(2010)3325-3330

[9] Y. L. Luo, L. H. Fan, F. Xu, Y. S. Chen, C. H. Zhang, Q.-B. Wei. Mater. Chem. Phys. 120(2011)590-597

[10] Z.M. Zhang, M.X. Wan, Y. Wei. Nanotechnology 16(2005)2827-2832

[11] X. Li, M.X. Wan, Y. Wei, J.Y. Shen, Z.J. Chen. J. Phys. Chem. B, 110(2006)14623-14626.

[12] S.B. Ni, S.M. Lin, Q.T. Pan, F. Yang, K. Huang, D.Y. He. J. Phys. D: Appl. Phys. 42(2009)055004.

[13] J. Deng, X. Ding, W. Zhang, Y. Peng, J.Wang, X. Long, P. Li, A. S. C. Chan, Polymer 43(2002) 2179–2184

[14] S. W. Phang, M. Tadokoro, J. Watanabe, N. Kuramoto. Polym. Adv. Technol. 20(2009) 550-557

[15] Y. Zhu, G.Q. Ren, M.X. Wan, L. Jiang. Macromol. Chem. Phys. 210(2009)2045-2051

[16] P. Jiang, J.F. Bertone, V.L. Colvin. Science 291(2001)453-457

[17] C.H. Yang, J.J. Du, Q. Peng, R.R. Qiao, W. Chen,C.L. Xu, Z.G. Shuai, M.Y. Gao. J. Phys. Chem. B, 113 (2009)5052–5058

[18]S.X. Xing, C. Zhao, T.L. Zhou, S.Y. Jing, Z.C. Wang. J. Appl. Polym. Sci. 104(2007) 3523-3529

[19] J.G. Deng, Y.X. Peng, C.L. He, X.P. Long, P. Li, A. S. C. Chan. Polym. Int. 52(2003) 1182-1187

[20] A.K. Bajpai, R. Gupta. Polym. Compos, 31(2010) 245-255

[21] W. Shen, M.M. Shi, M. Wang, H.Z. Chen. Mater. Chem. Phys. 112(2010)588-594

[22] S. E. Mavundla, G. F. Malgas, P. Baker, E. I. Iwuoha. Electroanalysis 20(2008)2347-2353

[23] C. He, C.H. Yang, Y.F. Li. Synth. Met. 139(2003)539-545

[24] A. C. V. De Araújo, Jr. S. Alves, W. M. Azevedo. Adv. Sci. Tech. 54(2008)325-330

[25] X.F. Lu, H. Mao, W.J. Zhang. Polym. Compos. 30(2009)847-854

[26]E.T. Kang, K.G. Neoh, K.L. Tan. Prog. Polym. Sci. 23(1998)277-324

[27] R. Gangopadhyay, A. De. Eur. Polym. J. 35(1999)1985-1992

[28] A.H. Chen, H.Q. Wang, B. Zhao, X.Y. Li. Synth. Met. 139(2003)411-415

[29] S.B. Ni, X.H. Wang, G. Zhou, F. Yang, J.M. Wang, D.Y. He. J. Alloys Compd. 489 (2010)252-256

[30] S.B. Ni, X.L. Sun, X.H. Wang, G. Zhou, F. Yang, J.M. Wang, D.Y. He. Mater. Chem.Phys., 124(2010)353-358

[31] X. L. Dong, X. F. Zhang, H. Huang, F. Zuo. Appl. Phys. Lett. 92(2008)013127-013127-3

[32] C. Kittel. Phys. Rev.73 (1948)155–161

[33] Z. Zou, A.G. Xuan, Z.G. Yan, Y.X. Wu, N. Li. Chem. Eng. Sci. 65(2010)160-164

[34] S.S. Kim, S.B. Jo, K.I. Gueon, K.K. Choi, J.M. Kim and K.S. Churn. IEEE Trans. Magn. 27(1991)5462-5464

[35] C.H. Yang, J.J. Du, Q. Peng, R.R. Qiao, W. Chen, C.L. Xu, Z.G. Shuai and M.Y. Gao. J. Phys. Chem. B, 113 (2009)5052–5058

[36] P. Xu, X.J. Han, J.J. Jiang, X.H. Wang, X.D. Li, and A.H. Wen. J. Phys. Chem. C 111(2007)12603-12608

[37] S.W. Phang, N. Kuramoto. Polym. Compos. 31(2010)516–523

**Figure captions:**

Figure 1. TEM image of $Fe_3O_4$ nanoparticles synthesized by co-precipitation (inset: corresponding enlarged TEM image).

Figure 2. Typical FE-SEM images, TEM images for (a, c) HPAP nanospheres and (b, d) HPAP-$Fe_{04}$ nanospheres.

Figure 3. XRD patterns of HPAP nanospheres, HPAP-$Fe_3O_4$ nanospheres with different amounts of $Fe_3O_4$ nanoparticles added, and $Fe_3O_4$ nanoparticles.

Figure 4. FT-IR spectra of $Fe_3O_4$ nanoparticles, HPAP nanospheres and HPAP-$Fe_3O_4$ nanospheres with different amounts of $Fe_3O_4$ nanoparticles added.

Figure 5. XPS spectra of (a) HPAP-$Fe_{04}$ nanospheres; (b) N 1s and (c) C 1s core level spectra of HPAP-$Fe_{04}$ nanospheres.

Figure 6. TGA curves for HPAP nanospheres and HPAP-$Fe_3O_4$ nanospheres with different amounts of $Fe_3O_4$ nanoparticles added.

Figure 7. Magnetization versus applied magnetic field at room temperature for the $Fe_3O_4$ nanoparticles and HPAP- $Fe_3O_4$ nanospheres

Figure 8. the relationship between saturated magnetization and $Fe_3O_4$ content in HPAP-$Fe_3O_4$ nanospheres.

Figure 9. Room temperature conductivity (σ) of the HPAP and HPAP- $Fe_3O_4$ nanospheres.

Figure 10. Permittivity and permeability of HPAP and HPAP- $Fe_3O_4$ nanospheres. (a) Real permittivity, $\varepsilon'$, (b) imaginary permittivity, $\varepsilon''$, (c) real permeability, $\mu'$ and (d) imaginary permeability, $\mu''$.

Figure 11. Frequency dependence of tan δ (tan $\delta_E$, tan $\delta_M$, tan $\delta_E$+tan $\delta_M$) for HPAP-$Fe_{04}$ composite.

Figure 12. Reflection loss curves for HPAP and HPAP-$Fe_3O_4$ nanospheres with 2 mm thickness in the frequency range of 0.5-10GHz

**TABLE 1** $Fe_3O_4$ contents in HPAP-$Fe_3O_4$ composite nanospheres obtained by TGA analysis

| **Samples** | **$Fe_2O_3$ Mass percentage (wt%)[a]** | **$Fe_3O_4$ content (wt%)[b]** |
|---|---|---|
| HPAP-$Fe_{01}$ | 4.0 | 3.87 |
| HPAP-$Fe_{02}$ | 6.4 | 6.19 |
| HPAP-$Fe_{04}$ | 20.0 | 19.33 |
| HPAP-$Fe_{06}$ | 22.0 | 21.27 |

[a] $Fe_2O_3$ mass percentage (wt %) measured through TGA analysis.

[b] $Fe_3O_4$ content in HPAP- $Fe_3O_4$ nanospheres calculated from the $Fe_2O_3$ mass percentage.

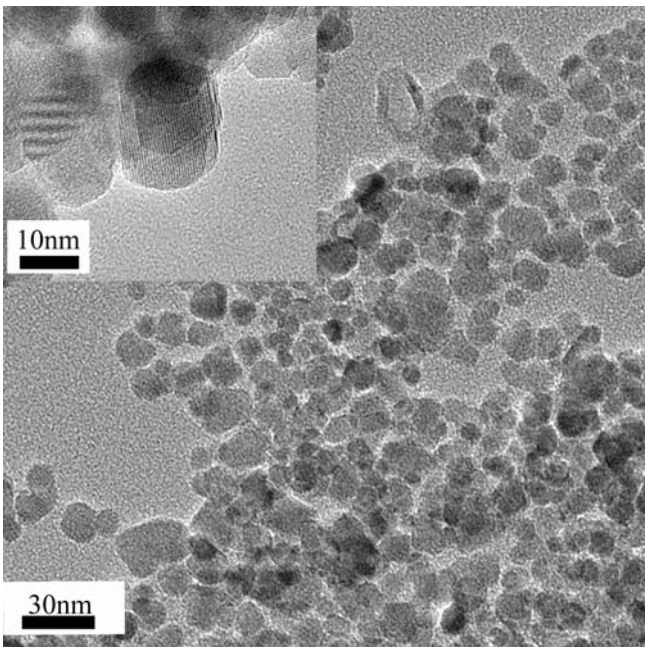


Figure 1.

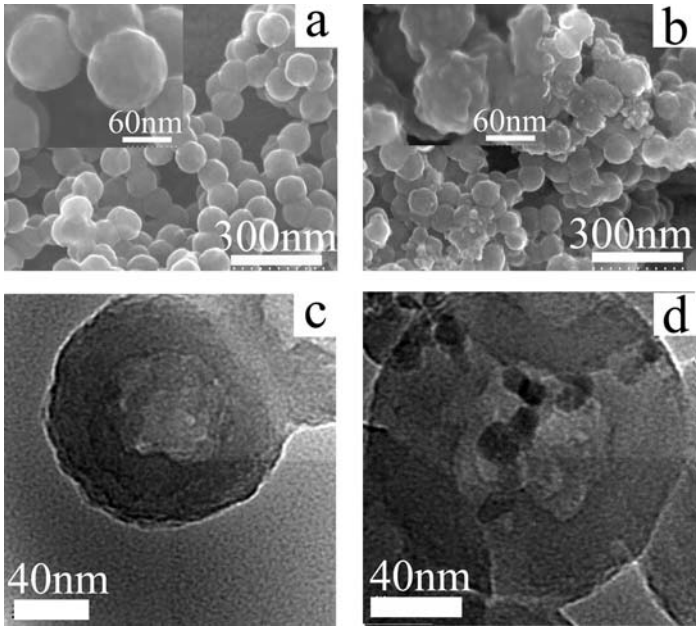


Figure 2.

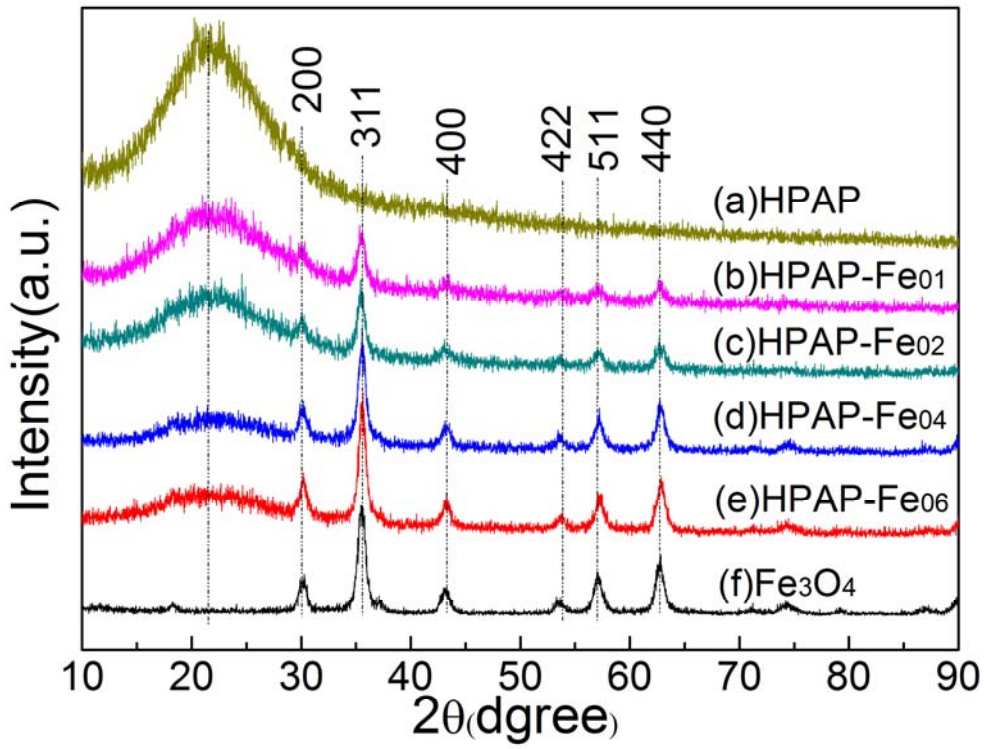
200
311
400
422
511
440
(a)HPAP
(b)HPAP-Fe01
(c)HPAP-Fe02
(d)HPAP-Fe04
(e)HPAP-Fe06
(f)Fe3O4
Intensity(a.u.)
10
20
30
40
50
60
70
80
90
2θ(dgree)

Figure 3.

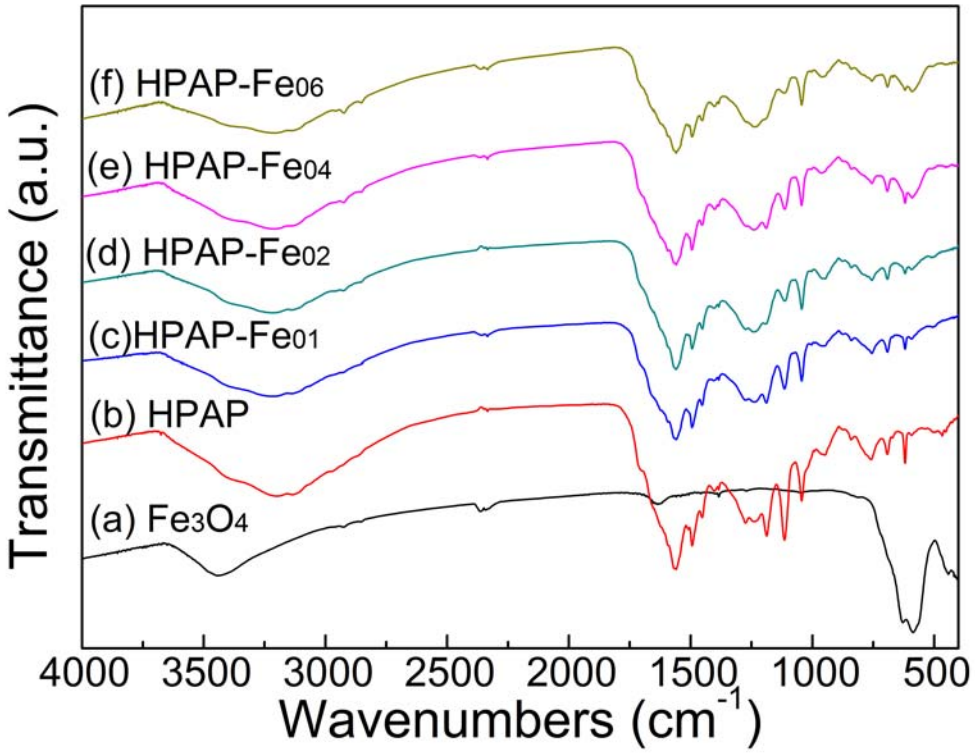
(f) HPAP-Fe06
(e) HPAP-Fe04
(d) HPAP-Fe02
(c)HPAP-Fe01
(b) HPAP
(a) Fe3O4
Transmittance (a.u.)
4000 3500 3000 2500 2000 1500 1000 500
Wavenumbers (cm-1)

Figure 4.

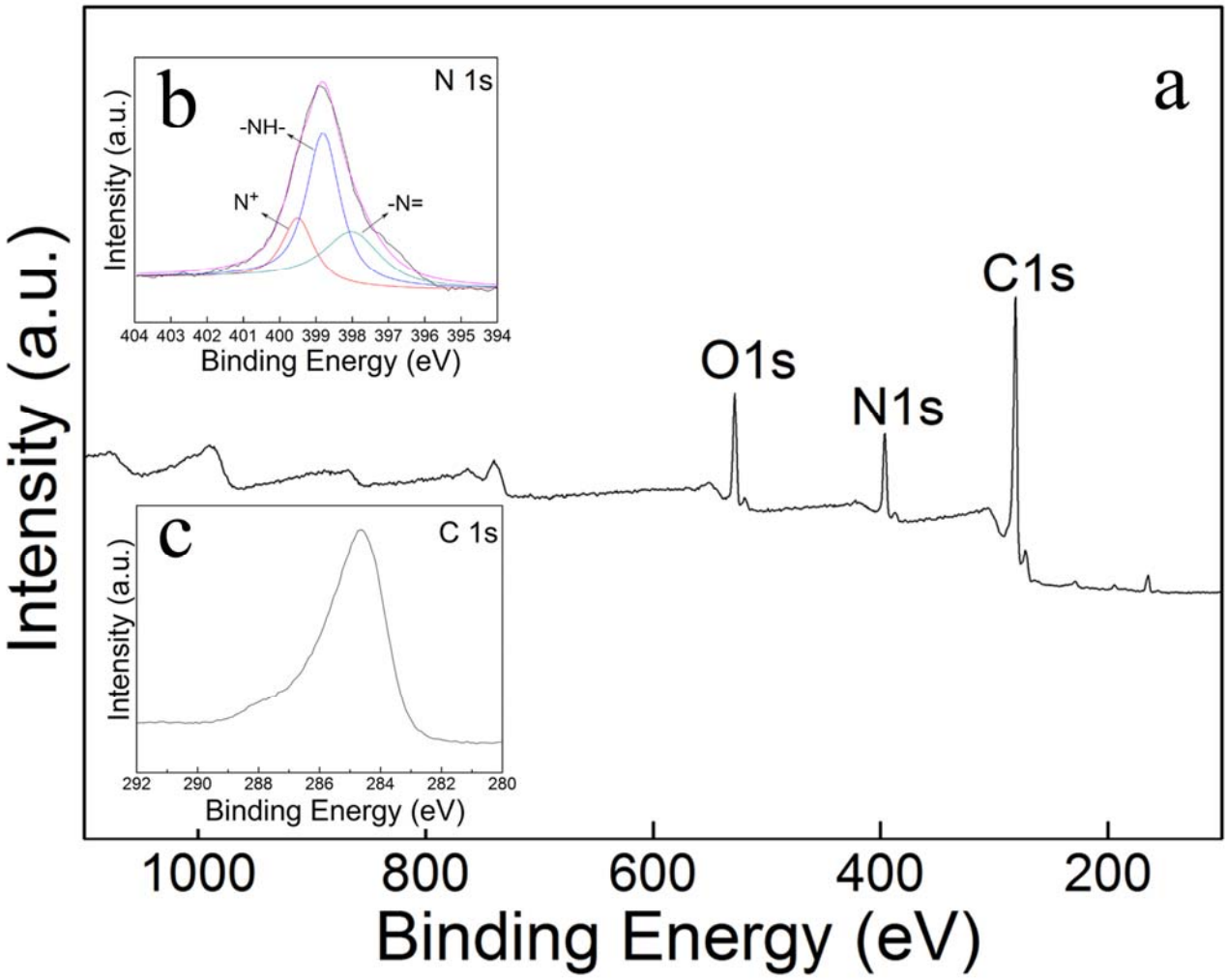
a
b
N 1s
-NH-
N+
-N=
Intensity (a.u.)
404 403 402 401 400 399 398 397 396 395 394
Binding Energy (eV)
c
C 1s
Intensity (a.u.)
292 290 288 286 284 282 280
Binding Energy (eV)
O1s
N1s
C1s
Intensity (a.u.)
1000 800 600 400 200
Binding Energy (eV)

Figure 5.

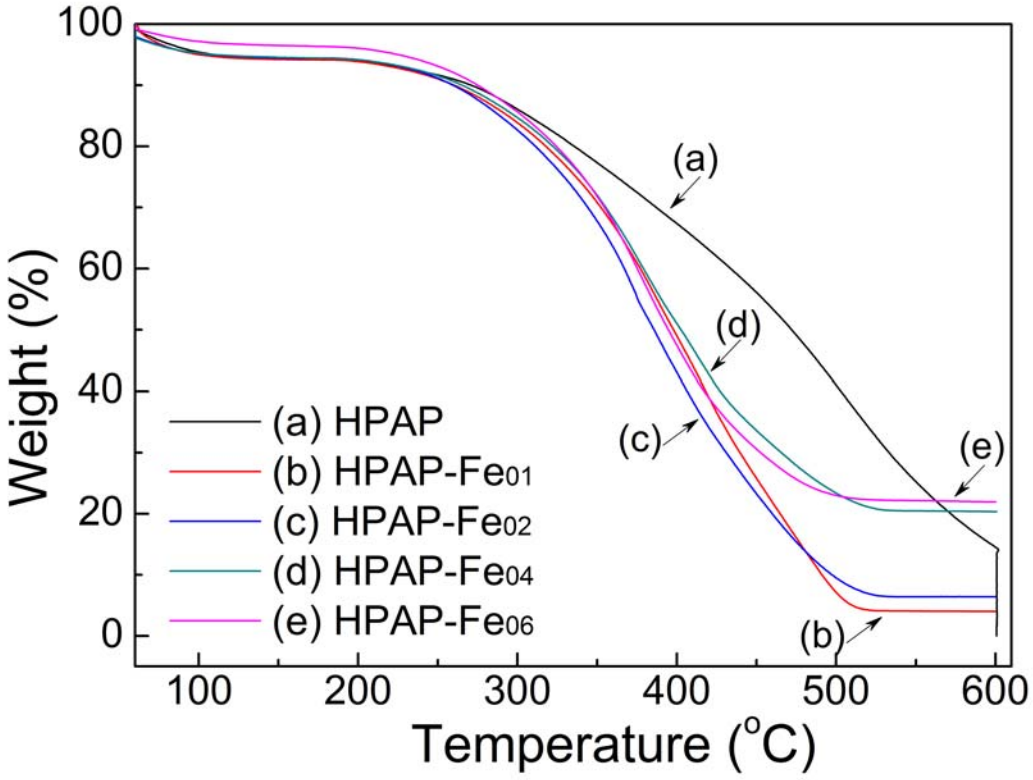
100
80
60
40
20
0
Weight (%)
100
200
300
400
500
600
Temperature (°C)
(a) HPAP
(b) HPAP-Fe01
(c) HPAP-Fe02
(d) HPAP-Fe04
(e) HPAP-Fe06
(a)
(b)
(c)
(d)
(e)

Figure 6.

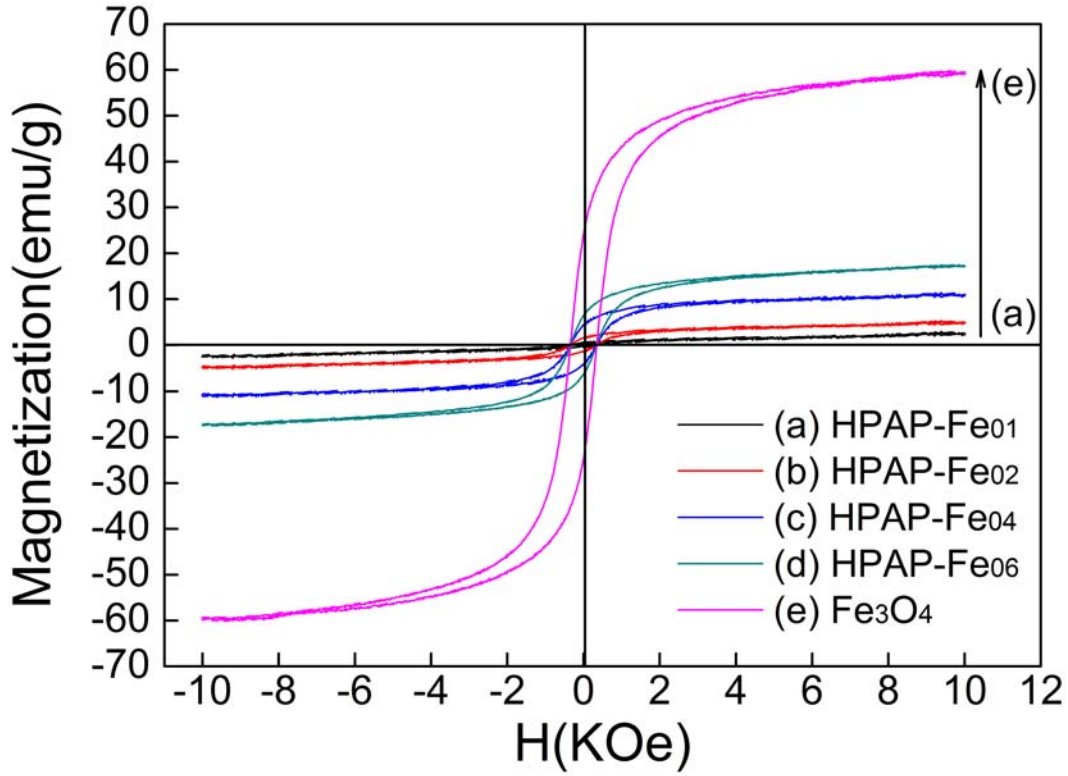
Magnetization(emu/g)
H(KOe)
(e)
(a)
(a) HPAP-Fe01
(b) HPAP-Fe02
(c) HPAP-Fe04
(d) HPAP-Fe06
(e) Fe3O4

Figure 7.

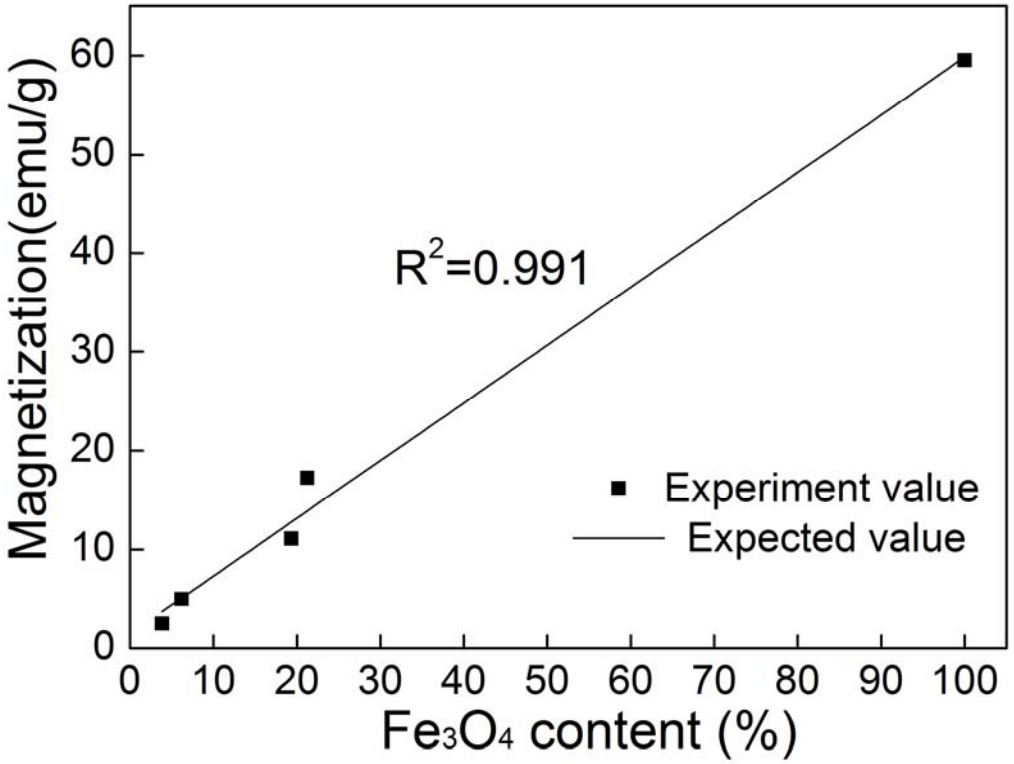
Magnetization(emu/g)
0
10
20
30
40
50
60
$R^2$=0.991
Experiment value
Expected value
0
10
20
30
40
50
60
70
80
90
100
$Fe_3O_4$ content (%)

Figure 8.

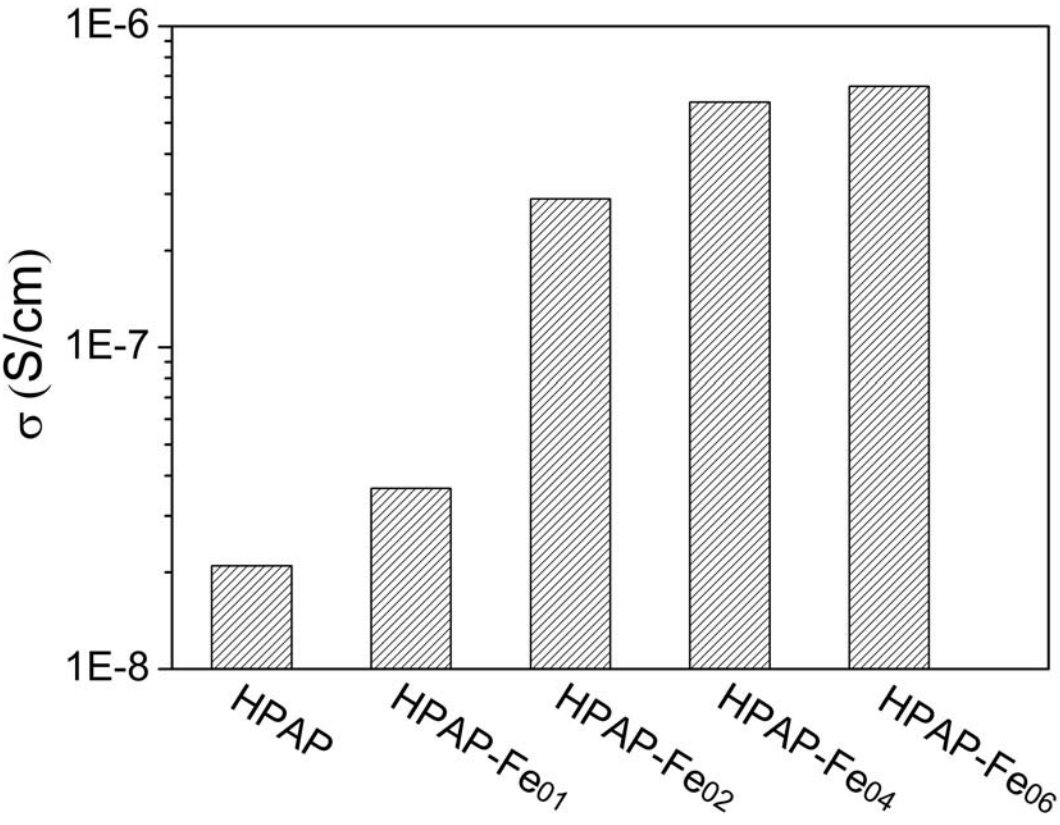


Figure 9.

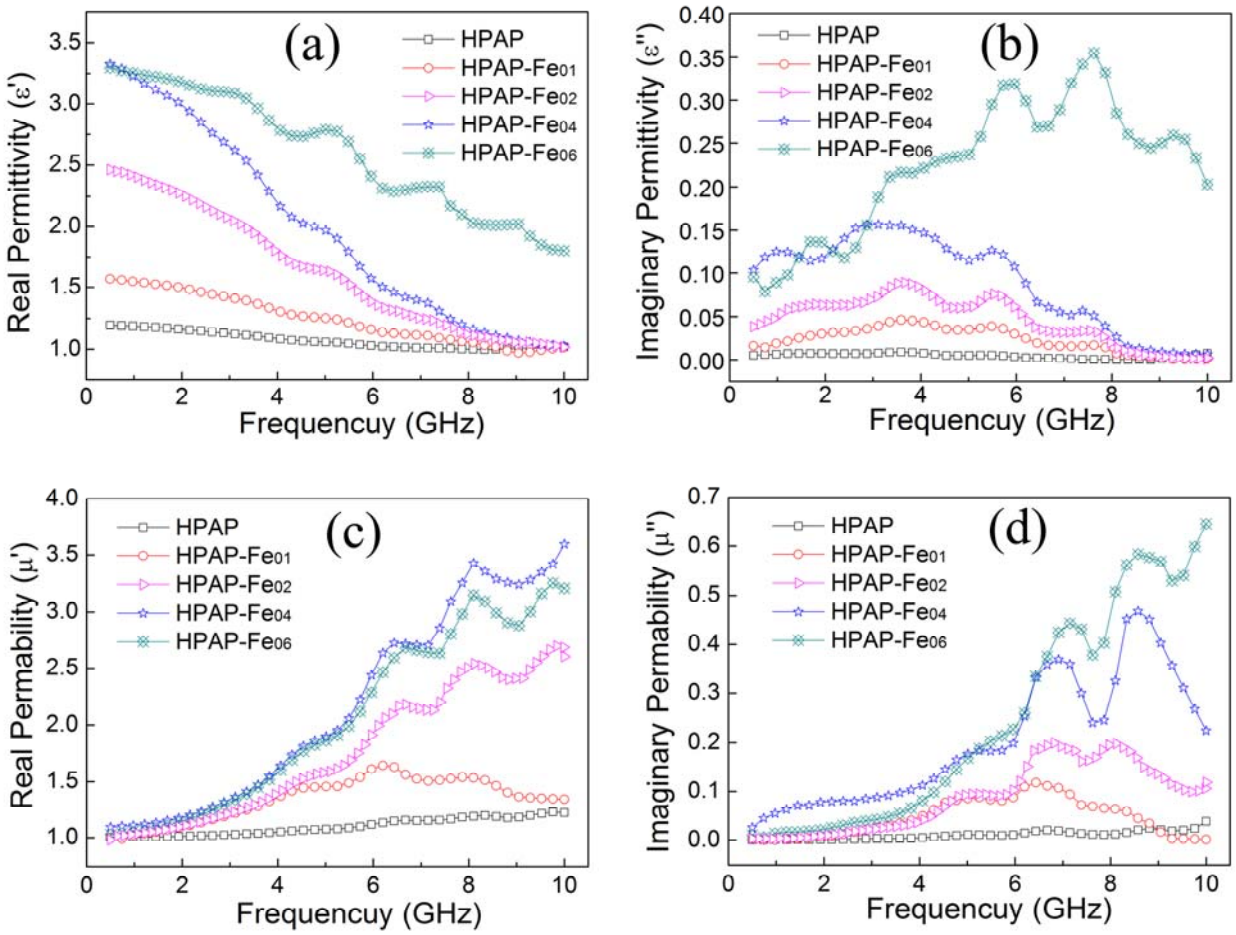
(a)
Real Permittivity (ε')
Frequencuy (GHz)
HPAP
HPAP-Fe01
HPAP-Fe02
HPAP-Fe04
HPAP-Fe06
(b)
Imaginary Permittivity (ε")
Frequencuy (GHz)
(c)
Real Permability (μ')
Frequencuy (GHz)
(d)
Imaginary Permability (μ")
Frequencuy (GHz)

Figure 10.

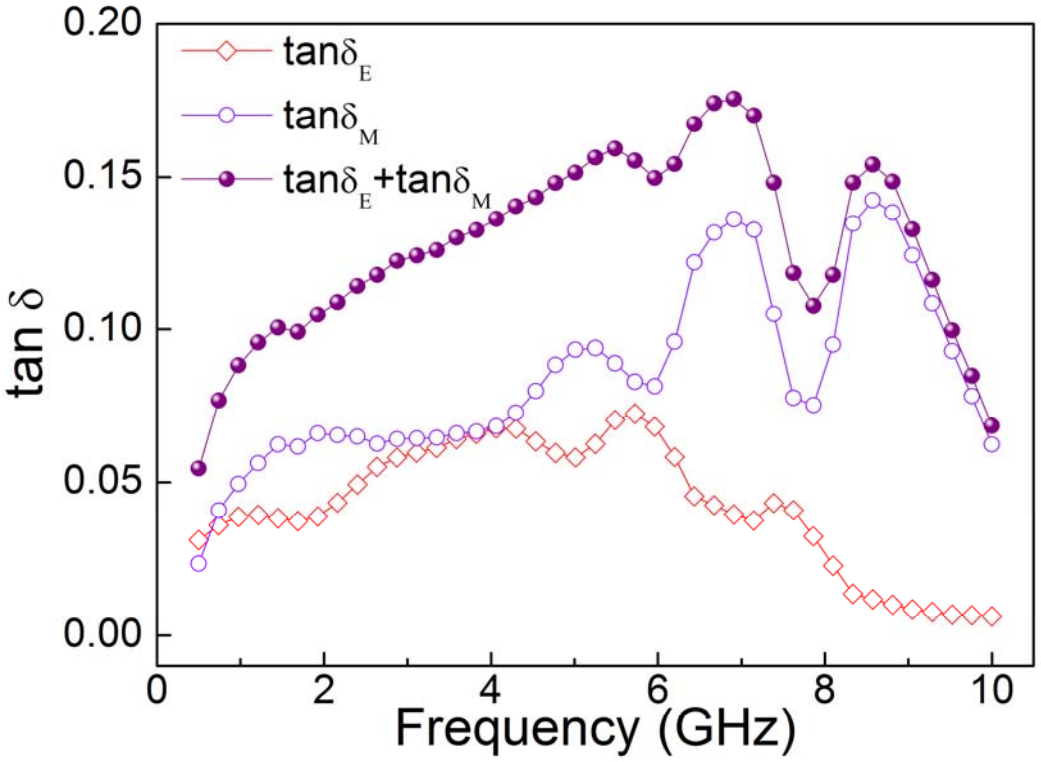
0.20
0.15
0.10
0.05
0.00
tan δ
tanδ_E
tanδ_M
tanδ_E+tanδ_M
0
2
4
6
8
10
Frequency (GHz)

Figure 11.

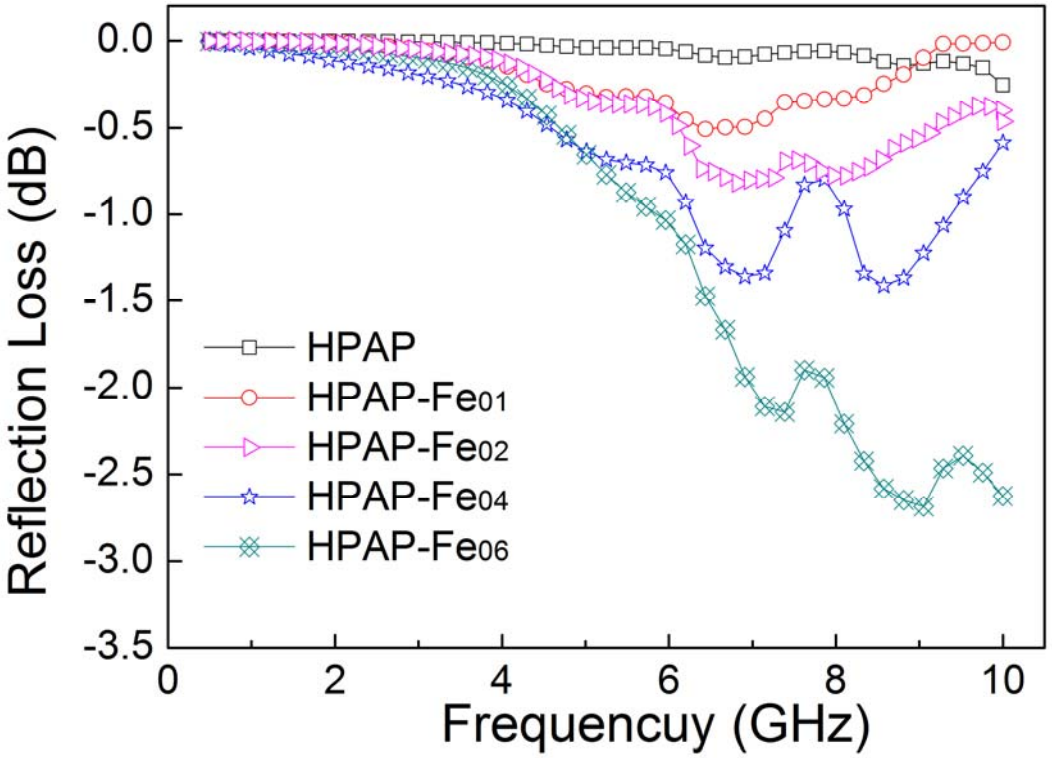
Reflection Loss (dB)
0.0
-0.5
-1.0
-1.5
-2.0
-2.5
-3.0
-3.5
0
2
4
6
8
10
Frequencuy (GHz)
HPAP
HPAP-Fe01
HPAP-Fe02
HPAP-Fe04
HPAP-Fe06

Figure 12.